Sensors & Diagnostics

PAPER

View Article Online
View Journal | View Issue

Check for updates

Cite this: *Sens. Diagn.*, 2023, **2**, 1649

A simple copper(II) dppy-based receptor for sensing of L-cysteine and L-histidine in aqueous acetonitrile medium†

Dipankar Das, [a] Aritra Roy, ‡[b] Sourav Sutradhar, [a] Felipe Fantuzzi *[c] and Biswa Nath Ghosh *[a]

Received 18th July 2023,
Accepted 19th October 2023

DOI: 10.1039/d3sd00183k

rsc.li/sensors

The development of simple yet efficient receptors that rapidly detect and monitor amino acids with high sensitivity and reliability is crucial for the early-stage identification of various diseases. In this work, we report the synthesis and characterisation of a copper(II) complex, $CuCl_2L$, by employing a 2,6-dipyrazinylpyridine (dppy)-based ligand (L = 2,2′-(4-(3,4,5-trimethoxyphenyl)pyridine-2,6-diyl) dipyrazine). The *in situ* prepared $CuCl_2L$ receptor exhibits an instantaneous response to the presence of L-cysteine (Cys) and L-histidine (His) in aqueous acetonitrile (4 : 1 v/v, 10 mM HEPES buffer, pH 7.4). Furthermore, competitive experiments demonstrate the selectivity of $CuCl_2L$ towards Cys (1 equiv.) in the vicinity of other L-amino acids in the aforementioned solvent conditions. The detection limits for Cys and His are calculated as 0.33 μM and 1.40 μM, respectively. DFT calculations offer a plausible explanation for the observed selectivity of the $CuCl_2L$ receptor towards Cys and His. They reveal that the most stable conformer of Cu : Cys complex (1 : 1) is a five-membered ring formed through *N*,*S*-coordination mode (ΔG = −26.7 kcal mol^{-1}) over various other possible coordination modes, while comparable ΔG values are only obtained for Cu : His complexes featuring two His moieties.

Open Access Article. Published on 21 October 2023. Downloaded on 12/9/2025 6:06:02 PM.
This article is licensed under a Creative Commons Attribution-NonCommercial 3.0 Unported Licence.

Introduction

L-Cysteine (Cys), one of the three naturally occurring biothiols, is a crucial amino acid that acts as an antioxidant to protect cells and tissues from oxidation by free radicals and reactive oxygen species.[1,2] It is also the only amino acid that participates in peptide and protein biosynthesis and plays a key role in enzyme-active sites.[2–5] The deficiency of Cys can lead to various health issues, such as liver damage,[6] hair depigmentation,[7] skin lesions,[8] edema,[9] lethargy,[10] child growth retardation,[11] and so on. In turn, an elevated level of Cys can result in neurological,[12] and cardiovascular diseases.[13,14] L-Histidine (His), another essential amino acid, performs vital functions in the nervous system,[15] including serving as a neurotransmitter,[16] and promoting tissue growth and repair.[17] His deficiency can lead to kidney disease,[18] Parkinson's disease,[19] epilepsy,[20] and other disorders. On the other hand, an elevated level of His can result in liver cirrhosis,[21] asthma,[22] and other conditions.[23]

Designing a receptor with a fast response, high sensitivity, and reliability for detecting and monitoring Cys and His concentrations can potentially aid in the early-stage recognition of various diseases.[24–28] In this context, several receptor analogues have been proposed for Cys and His recognition, including Schiff base,[29] 1,8-naphthalimide,[30] benzothiazole,[31] coumarin,[32] fluorescein,[33] BODIPY,[34] α,β-unsaturated ketone,[35] rhodamine,[36] imidazole,[37] nanomaterials based receptors,[38] metal–organic frameworks (MOFs),[39] *etc.* Various detection techniques have been employed for Cys and His detection, such as UV-visible spectroscopy,[40,41] fluorescence spectroscopy,[42] flow injection,[43] capillary electrophoresis,[44] Raman microspectroscopy,[45] liquid chromatography,[46] voltametric,[47] mass spectrometry,[48] *etc.* Recently, nitrogen-based heterocyclic ligands such as 2,2′:6′,2″-terpyridine, 2,6-dipyrazinylpyridine (dppy), and their transition metal complexes have garnered significant attention due to their easy one-pot synthesis, high stability, fascinating electrochemical and photophysical properties, and potential physiological activities.[49–53] These ligands have been incorporated into various applications, including self-assembly,[54] hydrogelation,[55–57] halogen bonding,[58,59] and anion sensing,[60,61] *etc.*

[a] *Department of Chemistry, National Institute of Technology Silchar, Silchar-788010, Assam, India. E-mail: bnghosh@che.nits.ac.in; Tel: +91 801 812 3682*
[b] *Department of Chemistry, Pondicherry University, Pondicherry 605014, India*
[c] *School of Chemistry and Forensic Science, University of Kent, Park Wood Rd, Canterbury CT2 7NH, UK. E-mail: f.fantuzzi@kent.ac.uk*

† Electronic supplementary information (ESI) available. See DOI: https://doi.org/10.1039/d3sd00183k

‡ Current Address: Department of Chemical and Energy Engineering, London South Bank University, 103 Borough Road, London SE1 0AA, UK.

© 2023 The Author(s). Published by the Royal Society of Chemistry

Open Access Article. Published on 21 October 2023. Downloaded on 12/9/2025 6:06:02 PM.
This article is licensed under a Creative Commons Attribution-NonCommercial 3.0 Unported Licence.

Most of the existing receptor analogues (non-metal complexes) for Cys sensing suffer from severe disadvantages, including laborious synthetic processes[30,31,34–36,62,63] and high response time.[33,64–66] Very few receptor systems (based on metal complexes, especially copper) reported Cys and His sensing over other L-amino acids, with a low detection limit and response time; however, the exact binding interaction mode of Cys with copper complexes has not been provided.[1,9,104] Herein, we present a novel copper(II) complex (**$CuCl_2L$**) featuring a one-pot, readily synthesisable dppy-based ligand (**L** = 2,2′-(4-(3,4,5-trimethoxyphenyl)pyridine-2,6-diyl)dipyrazine). This complex is designed for the immediate sensing of Cys and His over sixteen other L-amino acids (1 equiv.), seventeen anions (10 equiv.), and nine metal ions (1 equiv.). The detection is achieved at physiological pH (7.4) in aqueous acetonitrile (4 : 1 v/v, 10 mM HEPES buffer) with a comparatively low detection limit for Cys (0.33 μM) and His (1.40 μM), respectively, as determined through absorption spectral analysis. Additionally, we have also conducted DFT studies to i) assess the potential displacement of Cu(II) from **$CuCl_2L$** for the sensing of Cys and His and ii) investigate the optimal binding modes of Cu(II) interaction with Cys and His in an aqueous acetonitrile medium. To the best of our knowledge, this is the first instance of a substituted 2,6-dipyrazinylpyridine (dppy) based receptor system reported for L-amino acid sensing.

Experimental section

Materials and methods

The spectroscopic and analytical grade chemicals used in the synthesis and spectral analyses were procured commercially. The ligand 2,2′-(4-(3,4,5-trimethoxyphenyl) pyridine-2,6-diyl)dipyrazine **L** has been prepared following the literature method.[67] 3000 Hyperion FT-IR spectrometer (Bruker), ECZ500R/S1 (JEOL), and G2-XS QTOF mass spectrometer (XEVO), Thermo Electron Flash EA 1112 series were used to obtain FT-IR, ^{1}H NMR and HRMS and CHN analysis respectively. A Motras Scientific UV plus MSGUI3.1.0 absorption spectrophotometer was used to record absorption spectra.

Preparation of L

To an ethanolic solution (20 mL) of 2-acetylpyrazine (1.221 g, 10 mmol), KOH pellets (0.561 g, 10 mmol) were added and stirred, followed by the addition of 3,4,5-trimethoxybenzaldehyde (0.981 g, 5 mmol) and aqueous ammonia solution (15 mL). Stirring the resultant mixture at room temperature for 8 hours yielded a crude precipitate, which was separated by filtration and washed with ethanol (50 mL). The precipitate was dissolved in chloroform (10 mL), and an excess of *n*-hexane (80 mL) was added to it to obtain the white precipitate of **L**. The precipitate was filtered, washed with *n*-hexane, and dried. Yield: 0.802 g (2 mmol, 40%). ^{1}H NMR (500 MHz, $CDCl_3$) δ/ppm: 3.93 (s, 3H), 4.00 (s, 6H), 7.02 (s, 2H), 8.65–8.68 (m, 6H), 9.87 (s, 2H). ^{13}C (125 MHz, $CDCl_3$) δ/ppm: 56.5, 61.13, 104.65, 119.87, 133.77, 139.44, 143.65, 143.77, 144.92, 150.81, 151.02, 153.89, 154.42. ESI-MS $[L + H]^+$ *m*/*z* 402.20. Anal. calcd. $C_{22}H_{19}N_5O_3$ (401.426 g mol^{-1}): C, 65.83; H, 4.77; N, 17.45. Found: C, 65.58; H, 4.72; N, 17.55.

Preparation of $CuCl_2L$

L (0.08 g, 0.2 mmol) was dissolved in dichloromethane (10 mL), and then 10 mL of ethanolic solution of copper chloride (0.027 g, 0.2 mmol) was added to it. Stirring the resultant mixture at room temperature for 2 hours afforded a green color precipitate. The precipitate was filtered off, washed with ethanol (20 mL) and diethyl ether (20 mL), and then dried to get the green-colored copper complex **$CuCl_2L$**. Yield: 0.085 g (85%). ESI-MS $[CuClL]^+$ *m*/*z* 499.0720. Anal. calcd. $C_{22}H_{19}Cl_2CuN_5O_3$ (535.872 g mol^{-1}): C, 49.31; H, 3.57; N, 13.07. Found: C, 49.10 H, 3.49; N, 13.15.

Preparation of analyte solutions for UV-vis absorption spectral study

An acetonitrile solution of **L** (200 μM, 25 mL), an aqueous solution of $CuCl_2$ (1 mM, 10 mL), and aqueous solutions of glycine (Gly) and eighteen L-amino acids, namely alanine (Ala), aspartic acid (Asp), histidine (His), arginine (Arg), asparagine (Asn), cysteine (Cys), glutamic acid (Glu), methionine (Met), lysine (Lys), isoleucine (Ile), serine (Ser), proline (Pro), tryptophan (Trp), phenylalanine (Phe), valine (Val), leucine (Leu), threonine (Thr), and tyrosine (Tyr) (1 mM, 50 mL) were prepared separately. The **$CuCl_2L$** receptor solution was prepared *in situ* by mixing **L** (200 μM, 6 mL) and $CuCl_2$ (1 mM, 1.2 mL), followed by dilution to an aqueous acetonitrile HEPES buffer (10 mM, 32 mL, pH 7.4).

Computational details

All quantum chemical calculations were conducted using the Gaussian 16, Revision C.01 program package.[68] Geometry optimisations were carried out using the PBE0[69,70] functional in combination with the D3(BJ) method[71,72] for dispersion corrections. The basis set employed for all atoms, except Cu, was def2-SVP, while the triple-zeta def2-TZVP basis set[73] was used for Cu. This specific combination of basis sets is denoted as bs1; thus, the corresponding level of theory is referred to as PBE0-D3(BJ)/bs1. For open-shell systems, the unrestricted Kohn–Sham formalism was employed. For the calculation of the free energy values, Gibbs corrections at the PBE0-D3(BJ)/bs1 level were applied to single point energy calculations by utilising the same PBE0-D3(BJ) method but with a larger basis set. Specifically, the def2-TZVP basis set was used for all atoms, except for Cu, where the quadruple-zeta def2-QZVP basis set was employed. This combination of basis sets is denoted as bs2. Solvation effects were incorporated using the solvent model based on density (SMD),[74] with a solvent mixture of 4 : 1 (v/v) water/acetonitrile considered in the calculations. The energy calculations were, therefore, performed at the SMD/PBE0-D3(BJ)/bs2 level of

© 2023 The Author(s). Published by the Royal Society of Chemistry

Open Access Article. Published on 21 October 2023. Downloaded on 12/9/2025 6:06:02 PM.
This article is licensed under a Creative Commons Attribution-NonCommercial 3.0 Unported Licence.

theory. A concentration correction of $\Delta G^{0\rightarrow *} = 1.89$ kcal mol^{-1} was applied to the free energy values of all species to account for the change in standard states when transitioning from the gas phase (1 atm) to the condensed phase (1 M).[75–77] This correction ensures an accurate description of associative and dissociative steps. All the optimised geometries were characterised as minima on the corresponding potential energy surfaces by performing vibrational frequency calculations, confirming only positive eigenvalues in the Hessian matrices. The selected levels of theory for geometry optimisation and free energy calculations were benchmarked against other DFT functionals and basis sets, consistently yielding similar results. To ensure the identification of the global minimum energy structures, different starting structures were considered for all geometries. Finally, time-dependent DFT (TD-DFT) calculations with 20 states were conducted to describe the electronic excitation features of **$CuCl_2$L**. The resulting data were further analysed using the Multiwfn 3.8 program.[78]

Results and discussion

The experimental protocol of preparation of **L** and its Cu(II) complex **$CuCl_2$L** are shown in Scheme S1 in the ESI† and Scheme 1, respectively. **L** and **$CuCl_2$L** have been characterised using ^{1}H NMR, HRMS, elemental analysis, ESR, FT-IR, and the corresponding spectra can be found in ESI† (Fig. S1–S8). While we could not obtain an X-ray crystal structure for **$CuCl_2$L**, we have carried out DFT calculations which suggest favourable formation of **$CuCl_2$L** from isolated **L** and $CuCl_2$ moieties in aqueous acetonitrile solution (ΔG: −32.9 kcal mol^{-1}). In **CuC_2L**, the Cu(II) interacts with three donor nitrogen atoms of **L**, resulting in a penta-coordinate complex with a distorted square-pyramidal geometry (angular structural index parameter, τ = 0.08).[79–82] Similar structures have been observed in the case of copper complexes with analogous ligands,[79,81–83] many of which have been fully characterised by X-ray diffraction analysis.

Compound **L** (200 μM, 300 μL) exhibits absorption maxima at 227 nm and 293 nm in aqueous acetonitrile (2 mL, 4 : 1 v/v, 10 mM HEPES buffer, pH 7.4) (Fig. 1). The absorption maximum at 293 nm corresponds to an n → π* transition.[67,84,85] The addition of one equiv. of aqueous $CuCl_2$ (1 mM, 60 μL) to the solution of **L** (200 μM, 300 μL) in aqueous acetonitrile (2 mL, 4 : 1 v/v, 10 mM HEPES buffer, pH 7.4) resulted in the appearance of a new absorption band at 350 nm (Fig. 1). The absorption band at 350 nm, attributed to a ligand-to-metal charge transfer (LMCT) transition,[86–88] indicates the *in situ* formation of copper(II) complex **$CuCl_2$L**. The stability constant of this complex is determined to be 7.285×10^4 M^{-1}, calculated from B–H plot (Fig. S9 and S10 in the ESI†). The assignment of these transitions is in agreement with our TD-DFT calculations (see ESI† for more details). Specifically, the charge density difference (CDD)[89–91] plot (Fig. 1) demonstrates that the band at 350 nm is primarily attributed to a Cl-to-Cu LMCT transition, accompanied by a minor contribution from ligand-to-ligand charge transfer. The findings from the interfragment charge transfer (IFCT) analysis[78] further support these results, revealing an overall charge transfer character of 82% for the 350 nm band. Within this, the Cl ligands contribute to 87% of the hole density, while Cu and the dppy ligand contribute 68% and 18% of the electron density, respectively.

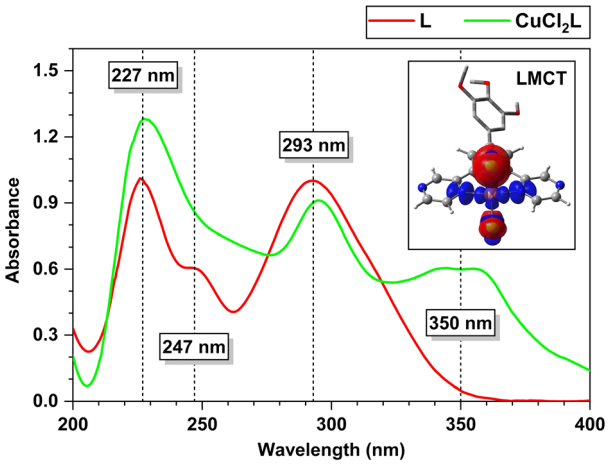

Fig. 1 Absorption spectra of **L** (red curve; 200 μM, 300 μL) and the *in situ* prepared **$CuCl_2$L** (green curve; 200 μM, 300 μL) in aqueous acetonitrile (2 mL, 4 : 1 v/v, 10 mM HEPES buffer, pH 7.4). Inset: charge density difference (CDD) plot of the LMCT transition of **$CuCl_2$L** at the SMD/ωB97X-D/bs2 level of theory. Charge flows from red to blue.

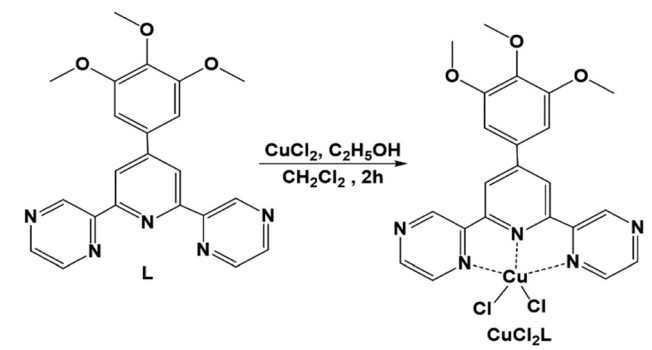

Scheme 1 Synthesis of **$CuCl_2$L**.

Aqueous solutions of Gly and various L-amino acids (Ala, Asp, His, Arg, Asn, Cys, Glu, Met, Lys, Ile, Ser, Pro, Trp, Val, Leu, Phe, Thr, and Tyr) at a concentration of 1 mM (60 μL) were individually added to solutions of the *in situ* prepared **$CuCl_2$L** (30 μM, 2 mL) in aqueous acetonitrile (4 : 1 v/v, 10 mM HEPES buffer, pH 7.4), and the corresponding absorption spectra were recorded. It was observed that the absorption spectrum of the copper(II) complex (**$CuCl_2$L**) remained unchanged upon the addition of most amino acid solutions, except for Cys and His (see Fig. 2). Specifically, when one equiv. of Cys was added to the copper complex solution, the 350 nm absorption band of **$CuCl_2$L** disappeared, resulting in absorption spectra closely resembling that of the free ligand **L** (Fig. 2). This suggests

Open Access Article. Published on 21 October 2023. Downloaded on 12/9/2025 6:06:02 PM.
This article is licensed under a Creative Commons Attribution-NonCommercial 3.0 Unported Licence.

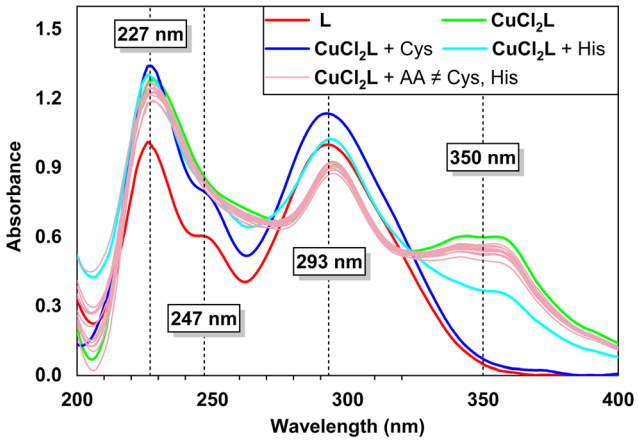

Fig. 2 Absorption spectra of the *in situ* prepared **$CuCl_2L$** (30 μM, 2 mL) upon addition of different amino acids (1 mM, 60 μL) in aqueous acetonitrile (4 : 1 v/v, 10 mM HEPES, pH 7.4). AA stands for amino acid.

that Cys displaced $CuCl_2$ from the **$CuCl_2L$** receptor previously formed upon adding **L** to the copper solution. Additionally, the 350 nm absorption band of **$CuCl_2L$** underwent a hypochromic shift when one equiv. of His was added to the receptor solution (Fig. 2), indicating the sensitivity of **$CuCl_2L$** towards His, along with Cys. Notably, almost 4 equiv. of His (1 mM, ~200 μL) were required to perturb the 350 nm absorption band of **$CuCl_2L$** completely. Furthermore, the detection study showed that *in situ* prepared **$CuCl_2L$** is most effective in the pH range of 4 to 9 for Cys detection, while pH 6.5 to 9 is most effective for His (1 equiv.) sensing (see details in Fig. S13 in the ESI†).

A UV-vis absorption spectral titration was carried out by gradually adding an aqueous solution of Cys (0.2 mM, 6 μL) to the *in situ* prepared **$CuCl_2L$** receptor (30 μM, 2 mL) in aqueous acetonitrile (4 : 1 v/v, 10 mM HEPES, pH 7.4). The absorption band at 293 nm of **$CuCl_2L$** exhibited gradual hyperchromic shifts, and the 350 nm absorption band underwent gradual hypochromic shifts as Cys solution was added incrementally to the **$CuCl_2L$** receptor (see Fig. 3a, top left). The presence of an isosbestic point at 320 nm for the above titration indicated the existence of an equilibrium between the **$CuCl_2L$** receptor and free **L** along with the Cu : Cys moiety. Similar observations were made in a UV-vis absorption spectral titration conducted by gradually adding His (0.5 mM, 5 μL) to the **$CuCl_2L$** receptor (30 μM, 2 mL) (see Fig. 3, top right). Both absorption spectral titrations demonstrate the sensitivity of the **$CuCl_2L$** receptor towards minute changes in Cys and His concentrations. The detection limits[92–94] for Cys and His were calculated to be 0.33 μM and 1.40 μM, respectively, indicating the high sensitivity of the **$CuCl_2L$** receptor for these analytes. The linear relationships

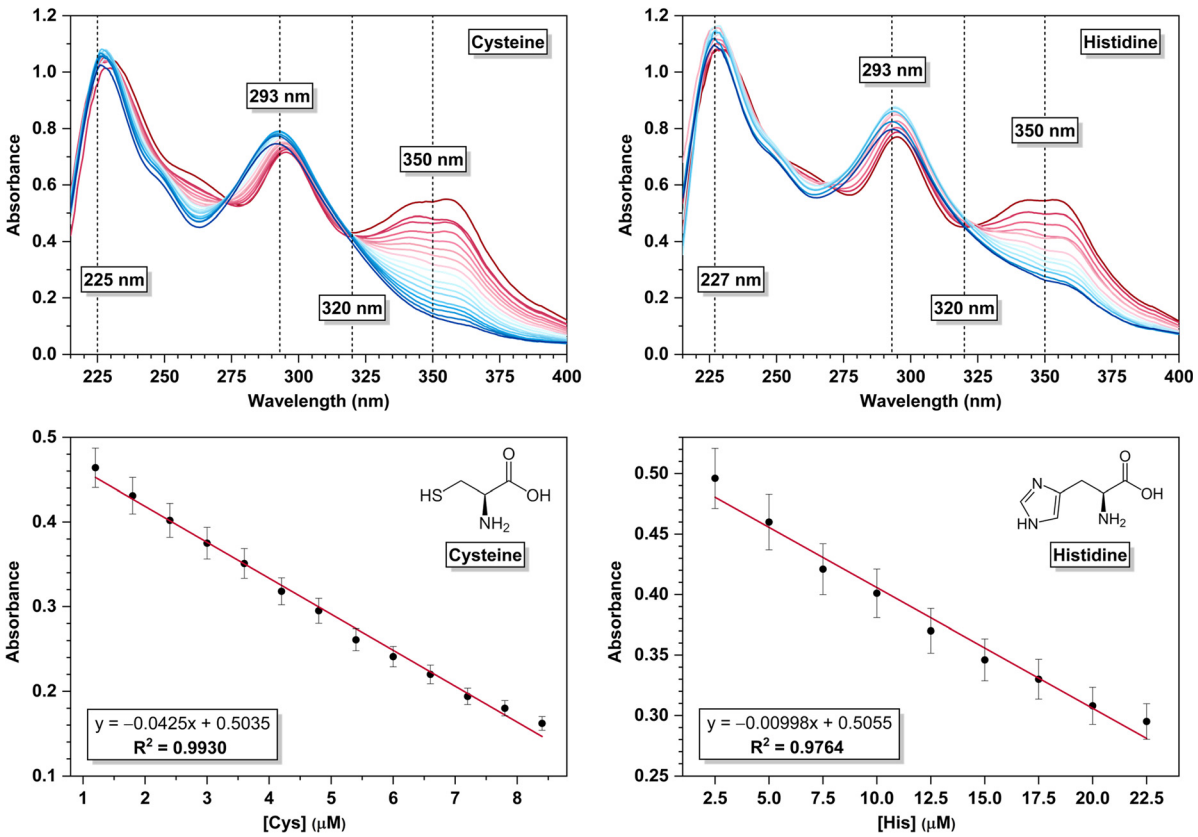

Fig. 3 Absorption spectra of the *in situ* prepared **$CuCl_2L$** (30 μM, 2 mL) upon gradual additions of (top left) Cys (0.2 mM, 6 μL) and (top right) His acids (0.5 mM, 5 μL) in aqueous acetonitrile (4 : 1 v/v, 10 mM HEPES, pH 7.4). Bottom: 350 nm absorption band intensity variation upon gradual addition of Cys (left) and His (right).

© 2023 The Author(s). Published by the Royal Society of Chemistry

Open Access Article. Published on 21 October 2023. Downloaded on 12/9/2025 6:06:02 PM.
This article is licensed under a Creative Commons Attribution-NonCommercial 3.0 Unported Licence.

found between the absorbance and concentration of Cys and His are shown in Fig. 3, bottom left and right, respectively.

To assess the selectivity of our receptor towards Cys, we conducted competition experiments, whose results are shown in Fig. 4. Initially, aqueous solutions of various amino acids (excluding Cys) at a concentration of 1 mM (60 μL) were individually added to distinct **$CuCl_2$L** solutions (30 μM, 2 mL) in aqueous acetonitrile (2 mL, 4 : 1 v/v, 10 mM HEPES buffer, pH 7.4), followed by the addition of one equiv. of Cys (1 mM, 60 μL) to each of these above mixtures. Interestingly, the 350 nm absorption band of **$CuCl_2$L**, which remained largely unaffected in the presence of other amino acids, disappeared upon addition of one equiv. of Cys. Similarly, when a mixture of different amino acids (60 μL) (excluding Cys) at a concentration of 1 mM was added collectively to the **$CuCl_2$L** solution (30 μM, 2 mL), followed by the addition of one equiv. of Cys (1 mM, 60 μL), we observed a similar outcome (see Fig. 4). These findings provide compelling evidence that the **$CuCl_2$L** receptor selectively detected Cys even in the presence of other L-amino acids.

To elucidate the selectivity mechanism of **$CuCl_2$L** towards Cys and His binding, we conducted additional DFT calculations (*vide supra*) on distinct Cu : Cys and Cu : His complexes. The results are summarised here, with more details given in the ESI.† Aligned with our experimental results, a 1 : 1 stoichiometric ratio was used for Cu : Cys complexes, while both 1 : 1 and 1 : 2 ratios were explored for Cu : His complexes. In our calculations, we considered that the SH and NH_3^+ groups of Cys undergo deprotonation upon metal binding, as observed in other metal–Cys complexes,[95] resulting in a doubly anionic $[Cys]^{2-}$ ligand. Indeed, our preliminary calculations considering the interaction of $CuCl_2$ with Cys at distinct charge states revealed that the complexes with doubly anionic $[Cys]^{2-}$ ligands are those with the most negative binding free energies (see Table S2 in the ESI† for further details). The $[Cys]^{2-}$ structure was obtained by considering the most stable zwitterionic form of Cys as described by Fernández-Ramos *et al.*[96] and removing the appropriate protons as the starting point for the geometry optimisation calculations. The most stable structure identified for $[Cys]^{2-}$ (**I**, see ESI†) was obtained through a systematic conformer search. This structure exhibits intramolecular N–H···O and N–H···S hydrogen bonds, which contribute to its stability. Notably, **I** is merely 0.4 kcal mol^{-1} more stable than that proposed by Foley and Enescu (**II**, see ESI†).[95]

Regarding the metal site, we examined both the bare, open-shell Cu(II) ion and the neutral, open-shell $CuCl_2$ moiety in our calculations. Consequently, we focused our investigations on the structure of [CuCys] and $[CuCysCl_2]^{2-}$ complexes. Whenever appropriate, we compared our [CuCys] results with those of $[CuCys]^{2+}$ by Belcastro and co-workers.[97] Regarding His, we only considered the R–$CH(NH_2)$–COO^- anionic state. As a result, we thoroughly examined the characteristics of $[CuHisCl_2]^-$ and $[Cu(His)_2]$ complexes. To explore the preference for chloride-bearing complexes in comparison to those without these ions, we conducted free energy calculations on a series of reactions (see ESI† for more details). Specifically, our results strongly indicate that the Cl groups remain bound to Cu following coordination with Cys, with the $[CuCysCl_2]^{2-}$ structure featuring the *N*,*S*-coordination (Fig. 5A) being the most stable one. This aligns well with the experimental data, which also supports the presence of such coordination. In turn, unlike Cys, our findings suggest that His exhibits a preference for forming complexes with the bare Cu(II) ion rather than $CuCl_2$. The most stable structure of $[Cu(His)_2]$ features a mixed configuration (Fig. 5B), where one His works as a tridentate ligand with *N*,*N*,*O*-coordination, and the other as a bidentate ligand through the amino and carboxyl groups (*N*,*O*-coordination). Our computational findings substantiate the observed differences in the stoichiometric ratio between copper cysteine and histidine complexes. Furthermore, they provide compelling evidence that the selectivity of **$CuCl_2$L** in amino acid sensing is attributed to the exceptionally stable coordination modes formed between $CuCl_2$ and the cysteine and histidine residues.

The detection limits and detection conditions achieved for Cys and His using the copper(II) complex in our work are

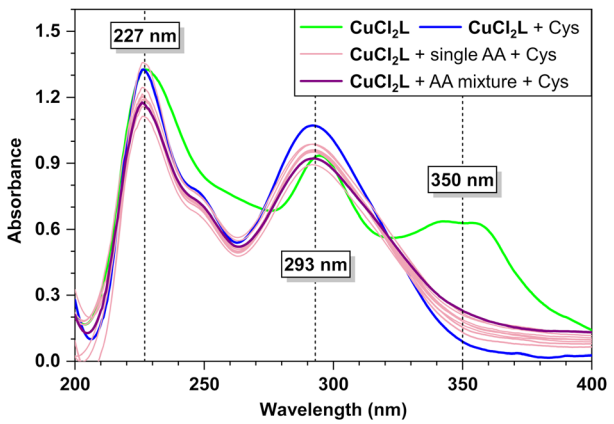

Fig. 4 Absorption spectra of *in situ* prepared **$CuCl_2$L** (30 μM, 2 mL) upon addition of different amino acids (1 mM, 60 μL) followed by the addition of one equiv. of Cys (1 mM, 60 μL) in aqueous acetonitrile (4 : 1 v/v, 10 mM HEPES, pH 7.4). AA stands for amino acid. In the single AA entries, only one amino acid different than Cys was added to the solution.

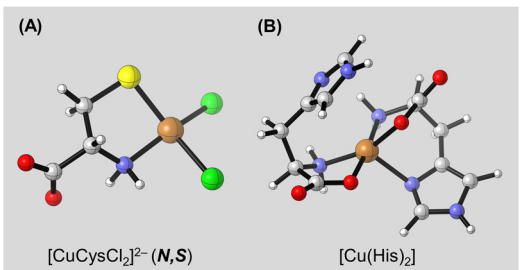

Fig. 5 Most stable structures of (A) $[CuCysCl_2]^{2-}$ and (B) $[Cu(His)_2]$ at the SMD/PBE0-D3(BJ)/bs2 level of theory. Geometries were optimised at the PBE0-D3(BJ)/bs1 level. For low-lying isomers, see Fig. S14 and S18 in the ESI.† Gray: carbon; white: hydrogen; red: oxygen; blue: nitrogen; green: chlorine; orange: copper.

Open Access Article. Published on 21 October 2023. Downloaded on 12/9/2025 6:06:02 PM. This article is licensed under a Creative Commons Attribution-NonCommercial 3.0 Unported Licence.

Table 1 Various analytical parameters of different receptor probes for Cys and His detection

Amino acid	Probe No.	Receptor probe	Conditions/detection medium	Detection limit (approx.)	Response time (approx.)	Ref.
L-Cysteine	01	Cu^{2+} based 4-(2-pyridylazo) resorcinol dye	H_2O	0.07 μM	30 s	1
	02	Cu^{2+} based zwitterionic chromophore dye	DMF	4.07 μM	10 s	9
	03	Chloropropionate-caged fluorescein probe	H_2O/DMSO (8 : 2, v/v, PBS, pH 7.4)	12.8 μM	10 min	33
	04	BODIPY-based receptor	CH_3CN/HEPES buffer (1 : 1, v/v, 20 mM, pH 7.4)	78 nM	20 min	98
	05	Two-photon fluorescent probe	DMF/PBS buffer (3 : 7, v/v, 10 mM, pH 7.4)	—	30 min	99
	06	Sulfonyl benzoxadiazole (SBD) dye having a chloride unit	DMF/PBS buffer (1 : 9, v/v, 10 mM, pH 7.4)	12.21 nM	20 min	100
	07	Imidazo[1,2-*a*]pyridine based probe having a acryloyl group	DMSO/HEPES buffer (8 : 2, v/v, pH 7.4)	0.33 μM	12 min	101
	08	Silver-ion-mediated Mg^{2+}-dependent DNAzyme	HEPES buffer (25 mM, pH 7.2) containing $NaNO_3$ (100 mM) and $Mg(NO_3)_2$ (10 mM)	2 nM	30 min	102
	09	Two-photon ratiometric fluorescent probe (DNEPI)	DMSO–PBS buffer (1 : 1, v/v, pH 7.4)	0.29 μM	2 min	103
	10	Imidazopyridine-based receptor	HEPES buffer (pH 7.34)	99 nM	Immediate	104
	11	Acrylate group-based dye	HEPES/DMSO buffer (19 : 1, v/v, 10 mM, pH 7.4)	0.16 μM	~3 min	105
	12	Boron dipyrromethene-based probe	CH_3CN/HEPES buffer (1 : 1, v/v, pH 7.4)	0.857 μM	30 min	64
	13	Flavone-based ESIPT ratiometric chemodosimeter	CH_3CN/HEPES buffer (10 mM, 1 : 1, v/v)	1 μM	60 min	65
	14	Fluorescein and rhodamine B-based chemosensor	CH_3CN/HEPES buffer (10 mM, 1 : 4, v/v, pH 7.4)	88 nM	20 min	106
	15	Nitroolefin-based coumarin	CH_3CN/HEPES buffer (0.1 M, 1 : 1, v/v, pH 7.4)	0.86 μM	0.5 min	107
	16	Styryl quinolinium/G-quadruplex complex	Tris-HAc buffer solution (pH 5)	2 nM	10 min	108
	17	AIE-based receptor (Schiff base)	HEPES buffer (10 mM, pH 7.4)	0.1 μM	3 min	109
	18	**Dppy-based Cu(II) receptor**	**CH_3CN/HEPES buffer (10 mM, 1 : 4, v/v, pH 7.4)**	**0.33 μM**	**Immediate**	**Present work**
L-Histidine	01	Oxidase-like activity of Cu(II) of *O*-phenylenediamine	CH_3CN (15%)/Tris–HCl buffer (50 mM pH 7.4)	0.33 μM	60 min	110
	02	Carbon quantum dots–Hg(II) system	PBS buffer (pH 6.0)	0.15 μM	2 min	111
	03	Copper nanoclusters	—	0.28 μM	4 min	112
	05	Doped zinc sulfide quantum dots	0.10 M PBS (pH 9.0)	0.74 μM	13 min	113
	06	Terbium(III) coordination polymer–copper(II) ensemble	NEM (5 mM, 10 μL) and HEPES buffer (100 mM, 10 μL, pH 7.4)	1.2 μM	20 min	114
	07	(*S*)-BINOL based receptor	^{i}PrOH/MeOH 99 : 1, v/v	70.3 nM	180 min	115
	08	**Dppy-based Cu(II) receptor**	**CH_3CN/HEPES buffer (10 mM, 1 : 4, v/v, pH 7.4)**	**1.40 μM**	**Immediate**	**Present work**

comparable to those reported in previous studies involving different receptor systems, as summarised in Table 1. These results highlight the effectiveness of our receptor in detecting and monitoring Cys and His. Moreover, our sensing studies demonstrate an immediate response time, notably faster than most previously reported systems. This rapid response further emphasises the efficiency and reliability of our copper(II) complex as a sensing tool for the identification of Cys and His in various applications.

Conclusions

In summary, we have synthesised and characterised a novel copper(II) complex, **$CuCl_2L$**, utilising a dppy-based ligand (**L** = 2,2′-(4-(3,4,5-trimethoxyphenyl)pyridine-2,6-diyl)dipyrazine). The *in situ* prepared **$CuCl_2L$** receptor exhibits rapid and sensitive detection of Cys and His amino acids in aqueous acetonitrile (4 : 1 v/v, 10 mM HEPES buffer, pH 7.4). Competitive experiments have demonstrated the selectivity of the **$CuCl_2L$** receptor towards Cys (1 equiv.) in the presence of other L-amino acids in the same solvent system. Notably, the detection limits for Cys and His were determined as 0.33 μM and 1.40 μM, respectively. These values are in line with those reported in previous studies utilising distinct receptors. Additionally, our sensing studies have demonstrated an exceptional response time, outperforming many existing systems. Our computational results strongly support the variations in the stoichiometric ratio observed in copper complexes with cysteine and histidine. Additionally, they strongly indicate that the remarkable selectivity of **$CuCl_2L$** in amino acid sensing originates the formation of highly stable coordination modes between $CuCl_2$ and the cysteine and histidine residues. These results underscore the promising potential of the **$CuCl_2L$** receptor as an efficient and reliable

© 2023 The Author(s). Published by the Royal Society of Chemistry

Open Access Article. Published on 21 October 2023. Downloaded on 12/9/2025 6:06:02 PM. This article is licensed under a Creative Commons Attribution-NonCommercial 3.0 Unported Licence.

tool for the early-stage identification and monitoring of Cys and His in various applications.

Author contributions

Dipankar Das: conceptualisation, investigation, formal analysis, data curation, writing – original draft. Aritra Roy: software, formal analysis, investigation. Sourav Sutradhar: methodology, data curation. Felipe Fantuzzi: conceptualisation, methodology, software, writing – original draft, writing – review & editing, supervision. Biswa Nath Ghosh: conceptualisation, validation, writing – original draft, writing – review & editing, supervision.

Conflicts of interest

There are no conflicts to declare.

Acknowledgements

F. F. acknowledges the University of Kent for financial and computational support. Special thanks are extended to Dr Timothy Kinnear for HPC assistance. D. D. acknowledges SAIF IIT Patna for providing NMR facility.

Notes and references

1 H. Tavallali, G. Deilamy-Rad, M. A. Karimi and E. Rahimy, *Anal. Biochem.*, 2019, **583**, 113376.
2 R. Zhang, J. Yong, J. Yuan and Z. Ping Xu, *Coord. Chem. Rev.*, 2020, **408**, 213182.
3 S. V. Mulay, Y. Kim, M. Choi, D. Y. Lee, J. Choi, Y. Lee, S. Jon and D. G. Churchill, *Anal. Chem.*, 2018, **90**, 2648–2654.
4 S. Muthusamy, L. Zhao, K. Rajalakshmi, D. Zhu, R. Soy, J. Mack, T. Nyokong, S. Wang, K. B. Lee and W. Zhu, *Dyes Pigm.*, 2021, **193**, 109556.
5 G. Zhao, W. Yang, F. Li, Z. Deng and Y. Hu, *J. Lumin.*, 2020, **226**, 117506.
6 U. Tamima, C. W. Song, M. Santra, Y. J. Reo, H. Banna, M. R. Islam and K. H. Ahn, *Sens. Actuators, B*, 2020, **322**, 128588.
7 Y. N. Wei, B. Lin, Y. Shu and J. H. Wang, *Analyst*, 2021, **146**, 4642–4648.
8 X. Yang, Y. Guo and R. M. Strongin, *Angew. Chem., Int. Ed.*, 2011, **50**, 10690–10693.
9 W. Hao, A. McBride, S. McBride, J. P. Gao and Z. Y. Wang, *J. Mater. Chem.*, 2011, **21**, 1040–1048.
10 Z. Li, Y. Zhang, Y. Jiang, H. Li, C. Chen and W. Liu, *J. Mater. Chem. B*, 2022, **10**, 6207–6213.
11 S. Shahrokhian, *Anal. Chem.*, 2001, **73**, 5972–5978.
12 J. P. Lomont and J. P. Smith, *Spectrochim. Acta, Part A*, 2022, **274**, 121068.
13 H. Huang, X. Ji, Y. Jiang, C. Zhang, X. Kang, J. Zhu, L. Sun and L. Yi, *Org. Biomol. Chem.*, 2020, **18**, 4004–4008.
14 L. El-Khairy, P. M. Ueland, H. Refsum, I. M. Graham and S. E. Vollset, *Circulation*, 2001, **103**, 2544–2549.
15 X. Huang, K. Li, X. Wang and P. Xia, *Spectrochim. Acta, Part A*, 2018, **205**, 287–291.
16 S. G. Eswaran, M. A. Ashkar, M. H. Mamat, S. Sahila, V. Mahalingam, H. V. S. R. M. Koppisetti and N. Vasimalai, *J. Sci.: Adv. Mater. Devices*, 2021, **6**, 100–107.
17 P. Munjal and H. M. Chawla, *J. Lumin.*, 2018, **203**, 364–370.
18 M. Watanabe, M. E. Suliman, A. R. Qureshi, E. Garcia-Lopez, P. Bárány, O. Heimbürger, P. Stenvinkel and B. Lindholm, *Am. J. Clin. Nutr.*, 2008, **87**, 1860–1866.
19 Q. Zhang, P. Zhang, S. Li, C. Fu and C. Ding, *Dyes Pigm.*, 2019, **171**, 107697.
20 T. Nagae, S. Aikawa, K. Inoue and Y. Fukushima, *Tetrahedron Lett.*, 2018, **59**, 3988–3993.
21 M. Chakraborty, M. Mohanty, R. Dinda, S. Sengupta and S. K. Chattopadhyay, *Polyhedron*, 2022, **211**, 115554.
22 G. Wei, F. Meng, Y. Wang, Y. Cheng and C. Zhu, *Macromol. Rapid Commun.*, 2014, **35**, 2077–2081.
23 P. Gunasekaran, C. I. David, S. Shanmugam, K. Ramanagul, R. Rajendran, V. Gothandapani, V. R. Kannan, J. Prabhu and R. Nandhakumar, *J. Agric. Food Chem.*, 2023, **71**, 802–814.
24 F. Yan, X. Sun, F. Zu, Z. Bai, Y. Jiang, K. Fan and J. Wang, *Methods Appl. Fluoresc.*, 2018, **6**, 42001.
25 Y. Wang, Q. Meng, Q. Han, G. He, Y. Hu, H. Feng, H. Jia, R. Zhang and Z. Zhang, *New J. Chem.*, 2018, **42**, 15839–15846.
26 S. Tajik, Z. Dourandish, P. M. Jahani, I. Sheikhshoaie, H. Beitollahi, M. Shahedi Asl, H. W. Jang and M. Shokouhimehr, *RSC Adv.*, 2021, **11**, 5411–5425.
27 Q. Meng, H. Jia, X. Gao, Y. Wang, R. Zhang, R. Wang and Z. Zhang, *Chem. – Asian J.*, 2015, **10**, 2411–2418.
28 Y. S. Kim, G. J. Park, S. A. Lee and C. Kim, *RSC Adv.*, 2015, **5**, 31179–31188.
29 T. Anand, A. S. K. Kumar and S. K. Sahoo, *Photochem. Photobiol. Sci.*, 2018, **17**, 414–422.
30 R. Shen, J. J. Yang, H. Luo, B. Wang and Y. Jiang, *Tetrahedron*, 2017, **73**, 373–377.
31 H. Li, L. Jin, Y. Kan and B. Yin, *Sens. Actuators, B*, 2014, **196**, 546–554.
32 X. Dai, Q. H. Wu, P. C. Wang, J. Tian, Y. Xu, S. Q. Wang, J. Y. Miao and B. X. Zhao, *Biosens. Bioelectron.*, 2014, **59**, 35–39.
33 D. P. Murale, H. Kim, W. S. Choi and D. G. Churchill, *RSC Adv.*, 2014, **4**, 5289–5292.
34 J. Shao, H. Guo, S. Ji and J. Zhao, *Biosens. Bioelectron.*, 2011, **26**, 3012–3017.
35 J. Li, Y. Yue, F. Huo and C. Yin, *Dyes Pigm.*, 2019, **164**, 335–340.
36 S. Y. Lim, D. H. Yoon, D. Y. Ha, J. M. Ahn, D. Il Kim, H. Kown, H. J. Ha and H. J. Kim, *Sens. Actuators, B*, 2013, **188**, 111–116.
37 B. Saha, P. Saha, A. Mandal, J. P. Naskar, D. Maiti and S. Chowdhury, *J. Chin. Chem. Soc.*, 2019, **66**, 506–514.
38 S. Yang and F. Liao, *Synth. Met.*, 2012, **162**, 1343–1347.
39 E. Lee, H. Ju, J. H. Jung, M. Ikeda, Y. Habata and S. S. Lee, *Inorg. Chem.*, 2019, **58**, 1177–1183.
40 M. R. Hormozi-Nezhad, E. Seyedhosseini and H. Robatjazi, *Sci. Iran.*, 2012, **19**, 958–963.
41 X. Li, K. Fan, X. Zhang, L. Wang, B. Qu and L. Lu, *Microchem. J.*, 2019, **146**, 486–491.

© 2023 The Author(s). Published by the Royal Society of Chemistry

Open Access Article. Published on 21 October 2023. Downloaded on 12/9/2025 6:06:02 PM.
This article is licensed under a Creative Commons Attribution-NonCommercial 3.0 Unported Licence.

42 S. C. Liang, H. Wang, Z. M. Zhang, X. Zhang and H. S. Zhang, *Spectrochim. Acta, Part A*, 2002, **58**, 2605–2611.
43 A. Waseem, M. Yaqoob and A. Nabi, *Curr. Pharm. Anal.*, 2013, **9**, 363–395.
44 J. S. Stamler and J. Loscalzo, *Anal. Chem.*, 1992, **64**, 779–785.
45 N. Cebi, C. E. Dogan, A. Develioglu, M. E. A. Yayla and O. Sagdic, *Food Chem.*, 2017, **228**, 116–124.
46 S. Wadud, M. M. Or-Rashid and R. Onodera, *J. Chromatogr. B: Anal. Technol. Biomed. Life Sci.*, 2002, **767**, 369–374.
47 A. Nezamzadeh-Ejhieh and H. S. Hashemi, *Talanta*, 2012, **88**, 201–208.
48 M. Rafii, R. Elango, G. Courtney-Martin, J. D. House, L. Fisher and P. B. Pencharz, *Anal. Biochem.*, 2007, **371**, 71–81.
49 D. Das, R. M. Gomila, P. Sarkar, S. Sutradhar, A. Frontera and B. N. Ghosh, *Polyhedron*, 2022, **223**, 115959.
50 B. N. Ghosh, F. Topić, P. K. Sahoo, P. Mal, J. Linnera, E. Kalenius, H. M. Tuononen and K. Rissanen, *Dalton Trans.*, 2015, **44**, 254–267.
51 S. Myadaraboina, M. Alla, V. Saddanapu, V. R. Bommena and A. Addlagatta, *Eur. J. Med. Chem.*, 2010, **45**, 5208–5216.
52 G. Ramesh, N. M. S. Kumar, P. R. Kumar, P. A. Suchetan, S. Devaraja, F. Sabine and G. Nagaraju, *J. Mol. Struct.*, 2020, **1200**, 127040.
53 K. Q. Wu, J. Guo, J. F. Yan, L. L. Xie, F. B. Xu, S. Bai, P. Nockemann and Y. F. Yuan, *Organometallics*, 2011, **30**, 3504–3511.
54 B. N. Ghosh, S. Bhowmik, P. Mal and K. Rissanen, *Chem. Commun.*, 2014, **50**, 734–736.
55 S. Sutradhar, S. Basak, D. Das and B. N. Ghosh, *Polyhedron*, 2023, **236**, 116344.
56 S. Bhowmik, B. N. Ghosh and K. Rissanen, *Org. Biomol. Chem.*, 2014, **12**, 8836–8839.
57 S. Sutradhar, D. Das and B. N. Ghosh, *J. Mol. Struct.*, 2022, **1265**, 133442.
58 D. Das, S. Sutradhar, K. Rissanen and B. N. Ghosh, *Z. Anorg. Allg. Chem.*, 2020, **646**, 301–306.
59 B. N. Ghosh, M. Lahtinen, E. Kalenius, P. Mal and K. Rissanen, *Cryst. Growth Des.*, 2016, **16**, 2527–2534.
60 S. Bhowmik, B. N. Ghosh, V. Marjomäki and K. Rissanen, *J. Am. Chem. Soc.*, 2014, **136**, 5543–5546.
61 D. Das, S. Sutradhar, A. Singh and B. N. Ghosh, *Z. Anorg. Allg. Chem.*, 2021, **647**, 1234–1238.
62 S. Manna, P. Karmakar, S. S. Ali, U. N. Guria, R. Sarkar, P. Datta, D. Mandal and A. K. Mahapatra, *New J. Chem.*, 2018, **42**, 4951–4958.
63 S. Manna, P. Karmakar, S. S. Ali, U. N. Guria, S. K. Samanta, R. Sarkar, P. Datta and A. K. Mahapatra, *Anal. Methods*, 2019, **11**, 1192–1198.
64 Q. Wu, Y. Wu, C. Yu, Z. Wang, E. Hao and L. Jiao, *Sens. Actuators, B*, 2017, **253**, 1079–1086.
65 B. Liu, J. Wang, G. Zhang, R. Bai and Y. Pang, *ACS Appl. Mater. Interfaces*, 2014, **6**, 4402–4407.
66 J. Wang, H. Wang, Y. Hao, S. Yang, H. Tian, B. Sun and Y. Liu, *Food Chem.*, 2018, **262**, 67–71.
67 R. Golla, P. R. Kumar, P. A. Suchethan, S. Foro and G. Nagaraju, *J. Mol. Struct.*, 2020, **1201**, 127118.
68 M. J. Frisch, G. W. Trucks, H. B. Schlegel, G. E. Scuseria, M. A. Robb, J. R. Cheeseman, G. Scalmani, V. Barone, B. Mennucci, G. A. Petersson, H. Nakatsuji, M. Caricato, X. Li, H. P. Hratchian, A. F. Izmaylov, J. Bloino, G. Zheng, J. L. Sonnenberg, M. Hada, M. Ehara, K. Toyota, R. Fukuda, J. Hasegawa, M. Ishida, T. Nakajima, Y. Honda, O. Kitao, H. Nakai, T. Vreven, J. A. Montgomery Jr., J. E. Peralta, F. Ogliaro, M. Bearpark, J. J. Heyd, E. Brothers, K. N. Kudin, V. N. Staroverov, R. Kobayashi, J. Normand, K. Raghavachari, A. Rendell, J. C. Burant, S. S. Iyengar, J. Tomasi, M. Cossi, N. Rega, J. M. Millam, M. Klene, J. E. Knox, J. B. Cross, V. Bakken, C. Adamo, J. Jaramillo, R. Gomperts, R. E. Stratmann, O. Yazyev, A. J. Austin, R. Cammi, C. Pomelli, J. W. Ochterski, R. L. Martin, K. Morokuma, V. G. Zakrzewski, G. A. Voth, P. Salvador, J. J. Dannenberg, S. Dapprich, A. D. Daniels, Ö. Farkas, J. B. Foresman, J. V. Ortiz, J. Cioslowski and D. J. Fox, *Gaussian 16, Revision C.01*, Gaussian, Inc., Wallingford CT, 2016.
69 C. Adamo and V. Barone, *J. Chem. Phys.*, 1999, **110**, 6158–6170.
70 M. Ernzerhof and G. E. Scuseria, *J. Chem. Phys.*, 1999, **110**, 5029–5036.
71 S. Grimme, J. Antony, S. Ehrlich and H. Krieg, *J. Chem. Phys.*, 2010, **132**, 154104.
72 S. Grimme, S. Ehrlich and L. Goerigk, *J. Comput. Chem.*, 2011, **32**, 1456–1465.
73 F. Weigend and R. Ahlrichs, *Phys. Chem. Chem. Phys.*, 2005, **7**, 3297–3305.
74 A. V. Marenich, C. J. Cramer and D. G. Truhlar, *J. Phys. Chem. B*, 2009, **113**, 6378–6396.
75 R. L. Martin, P. J. Hay and L. R. Pratt, *J. Phys. Chem. A*, 1998, **102**, 3565–3573.
76 M. Sparta, C. Riplinger and F. Neese, *J. Chem. Theory Comput.*, 2014, **10**, 1099–1108.
77 F. Fantuzzi, M. A. C. Nascimento, B. Ginovska, R. M. Bullock and S. Raugei, *Dalton Trans.*, 2021, **50**, 840–849.
78 T. Lu and F. Chen, *J. Comput. Chem.*, 2012, **33**, 580–592.
79 K. Choroba, B. Machura, S. Kula, L. R. Raposo, A. R. Fernandes, R. Kruszynski, K. Erfurt, L. S. Shul'Pina, Y. N. Kozlov and G. B. Shul'Pin, *Dalton Trans.*, 2019, **48**, 12656–12673.
80 A. W. Addison and T. N. Rao, *Polyhedron*, 1998, **17**, 1349–1356.
81 H. R. Khavasi and M. Esmaeili, *Cryst. Growth Des.*, 2019, **19**, 4369–4377.
82 L. Li, Y. Z. Zhang, C. Yang, E. Liu, J. C. Fettinger and G. Zhang, *J. Mol. Struct.*, 2016, **1110**, 19–23.
83 H. R. Khavasi and M. Esmaeili, *Langmuir*, 2019, **35**, 4660–4671.
84 F. A. Al-Mutlaq, P. G. Potvin, A. I. Philippopoulos and P. Falaras, *Eur. J. Inorg. Chem.*, 2007, 2121–2128.
85 M. Małecka, B. Machura and A. Szlapa-Kula, *Dyes Pigm.*, 2021, **188**, 109168.
86 X.-X. Han, X. Han, Y. Wang, D. Shang, Y.-H. Xing and F.-Y. Bai, *Polyhedron*, 2018, **151**, 192–198.

© 2023 The Author(s). Published by the Royal Society of Chemistry

Open Access Article. Published on 21 October 2023. Downloaded on 12/9/2025 6:06:02 PM.
This article is licensed under a Creative Commons Attribution-NonCommercial 3.0 Unported Licence.

87 R. Hao, L. Li, S. Zhu, Z.-H. Wang, X.-J. Zhao and E.-C. Yang, *J. Mol. Struct.*, 2019, **1176**, 376–385.
88 N. Zhang, J. Tang, Y. Ma, M. Liang, D. Zeng and G. Hefter, *Phys. Chem. Chem. Phys.*, 2021, **23**, 6807–6814.
89 T. Le Bahers, C. Adamo and I. Ciofini, *J. Chem. Theory Comput.*, 2011, **7**, 2498–2506.
90 D. Jacquemin, T. Le Bahers, C. Adamo and I. Ciofini, *Phys. Chem. Chem. Phys.*, 2012, **14**, 5383.
91 I. Ciofini, T. Le Bahers, C. Adamo, F. Odobel and D. Jacquemin, *J. Phys. Chem. C*, 2012, **116**, 11946–11955.
92 J. Xu, H. Li, L. Li, J. Wang, F. Wang and L. He, *J. Braz. Chem. Soc.*, 2020, **31**, 1778–1786.
93 D. Das, P. Sarkar, A. H. U. Kumar, S. Sutradhar, M. Kotakonda, N. K. Lokanath and B. N. Ghosh, *J. Photochem. Photobiol., A*, 2023, **441**, 114726.
94 D. Das, S. Sutradhar, R. M. Gomila, K. Rissanen, A. Frontera and B. N. Ghosh, *J. Mol. Struct.*, 2023, **1273**, 134269.
95 S. Foley and M. Enescu, *Vib. Spectrosc.*, 2007, **44**, 256–265.
96 A. Fernández-Ramos, E. Cabaleiro-Lago, J. M. Hermida-Ramón, E. Martínez-Núñez and A. Peña-Gallego, *J. Mol. Struct.: THEOCHEM*, 2000, **498**, 191–200.
97 M. Belcastro, T. Marino, N. Russo and M. Toscano, *J. Mass Spectrom.*, 2005, **40**, 300–306.
98 F. Wang, Z. Guo, X. Li, X. Li and C. Zhao, *Chem. – Eur. J.*, 2014, **20**, 11471–11478.
99 S. Yang, C. Guo, Y. Li, J. Guo, J. Xiao, Z. Qing, J. Li and R. Yang, *ACS Sens.*, 2018, **3**, 2415–2422.
100 K. B. Li, W. B. Qu, D. M. Han, S. Zhang, W. Shi, C. X. Chen and X. X. Liang, *Talanta*, 2019, **194**, 803–808.
101 M. Zhu, L. Wang, X. Wu, R. Na, Y. Wang, Q. X. Li and B. D. Hammock, *Anal. Chim. Acta*, 2019, **1058**, 155–165.
102 X. H. Zhao, L. Z. Zhang, S. Y. Zhao, X. H. Cui, L. Gong, R. Zhao, B. F. Yu and J. Xie, *Analyst*, 2019, **144**, 1982–1987.
103 L. Fan, W. Zhang, X. Wang, W. Dong, Y. Tong, C. Dong and S. Shuang, *Analyst*, 2019, **144**, 439–447.
104 S. Priyanga, T. Khamrang, M. Velusamy, S. Karthi, B. Ashokkumar and R. Mayilmurugan, *Dalton Trans.*, 2019, **48**, 1489–1503.
105 J. Zhang, J. Wang, J. Liu, L. Ning, X. Zhu, B. Yu, X. Liu, X. Yao and H. Zhang, *Anal. Chem.*, 2015, **87**, 4856–4863.
106 H. Chen, B. Zhou, R. Ye, J. Zhu and X. Bao, *Sens. Actuators, B*, 2017, **251**, 481–489.
107 Y. Q. Sun, M. Chen, J. Liu, X. Lv, J. F. Li and W. Guo, *Chem. Commun.*, 2011, **47**, 11029–11031.
108 Y. J. Lu, N. Ma, Y. J. Li, Z. Y. Lin, B. Qiu, G. N. Chen and K. Y. Wong, *Sens. Actuators, B*, 2012, **173**, 295–299.
109 L. Yan, Z. Kong, W. Shen, W. Du, Y. Zhou and Z. Qi, *RSC Adv.*, 2016, **6**, 5636–5640.
110 Y. Xu, X. Q. Wu, J. S. Shen and H. W. Zhang, *RSC Adv.*, 2015, **5**, 92114–92120.
111 J. Hou, F. Zhang, X. Yan, L. Wang, J. Yan, H. Ding and L. Ding, *Anal. Chim. Acta*, 2015, **859**, 72–78.
112 Q. Tan, J. Qiao, R. Zhang and L. Qi, *Microchem. J.*, 2020, **153**, 2–7.
113 W. Bian, F. Wang, Y. Wei, L. Wang, Q. Liu, W. Dong, S. Shuang and M. M. F. Choi, *Anal. Chim. Acta*, 2015, **856**, 82–89.
114 S. F. Xue, L. F. Lu, Q. X. Wang, S. Zhang, M. Zhang and G. Shi, *Talanta*, 2016, **158**, 208–213.
115 J. Tian, K. Lu, Y. Wang, Y. Chen, B. Huo, Y. Jiang, S. Yu, X. Yu and L. Pu, *Tetrahedron*, 2021, **95**, 132366.